# Positional information encoded in the dynamic differences between neighbouring oscillators during vertebrate segmentation.

Marcelo Boareto[1,2], Tomas Tomka[1] and Dagmar Iber[1,2,*]

**Affiliations**

[1] *Department of Biosystems Science and Engineering (D-BSSE), ETH Zurich, Mattenstrasse 26, 4058 Basel, Switzerland*

[2] *Swiss Institute of Bioinformatics, Mattenstrasse 26, 4058 Basel, Switzerland.*

*Correspondence to: dagmar.iber@bsse.ethz.ch

## Abstract

How cells track their position during the segmentation of the vertebrate body remains elusive. For decades, this process has been interpreted according to the clock-and-wavefront model, where molecular oscillators set the frequency of somite formation while the positional information is encoded in signaling gradients. Recent experiments using *ex vivo* explants challenge this interpretation, suggesting that positional information is encoded in the properties of the oscillators. Here, we propose that positional information is encoded in the differential levels of neighboring oscillators. The differences gradually increase because both the oscillator amplitude and the period increase with time. When this difference exceeds a certain threshold, the segmentation program starts. Using this framework, we quantitatively fit experimental data from *in vivo* and *ex vivo* mouse segmentation, and propose mechanisms of somite scaling. Our results suggest a novel mechanism of spatial pattern formation based on the local interactions between dynamic molecular oscillators.

## Introduction

Pattern formation during embryonic development requires that the cells assess their spatial position. One useful conceptual framework to understand this process is to assume that each cell has a positional value that relates to its position in the coordinate system. The cells then use this positional information to coordinate their differentiation process (Wolpert, 1969). Based on this conceptual framework, Cooke and Zeeman proposed a model to explain the sequential and periodic formation of the somites in the vertebrate embryo. In their model, the positional information of the cells is given by a signaling wavefront, while a clock sets the frequency of somite formation (Cooke and Zeeman, 1976).

The ‘clock-and-wavefront’ model guided much of the experimental work done in the subsequent decades. It has been shown that the rhythm of segmentation is established by travelling waves of gene expression, which sweep from the tail bud to the anterior end of the presomitic mesoderm (PSM) (Palmeirim et al., 1997). These waves emerge from the oscillatory expression of ‘clock’ genes involved in the Notch pathway, such as *Lfng* and *Hes* (McGrew et al 1998; Palmeirim et al., 1997; Forsberg et al, 1998; Dequeant et al., 2006; Niwa et al., 2007). In the tail bud region, where the PSM cells are generated, *Fgf8* and *Wnt3* are produced and as the cells cross the PSM their mRNA levels decrease due to degradation, creating a gradient by inheritance (Dubrulle and Pourquié 2004; Aulehla et al, 2003). Perturbations on Wnt and Fgf gradients have been shown to affect somite formation (Dubrulle et al, 2001; Sawada et al, 2001; Naiche et al 2011), therefore suggesting that these signaling gradients could in principle encode the wavefront of somite formation.

Recently, experiments of *ex vivo* explants have challenged the ‘clock-and-wavefront’ view and favored an interpretation where the wavefront is implicit in the dynamics of the clock (Lauschke et al, 2013). In these experiments, tail bud tissue is explanted and forms a monolayer PSM (mPSM) with concentric travelling waves sweeping from the center of a dish to its periphery. Interestingly, after growth stops, segments begin to form, and the size of the segments scales with the size of the mPSM (Lauschke et al 2013). The formation of these segments in the absence of growth cannot be easily explained with the ‘clock-and-wavefront’ model as it would require long-range mechanisms that sense the mPSM length. An alternative model was proposed where the wavefront is defined via the relative phase of a cellular oscillator compared to the tail bud oscillation (Lauschke et al., 2013). Since then, mechanistic networks that can compute such a relative phase of oscillation have been investigated (Beaupeux and François, 2016). A possible explanation includes two signaling oscillators in each cell and the phase shift between these oscillators would determine segmentation (Lauschke et al., 2013; Beaupeux and François, 2016, Sonnen et al, 2018). However, how these oscillators would control *in vivo* segmentation remains unclear.

The *Hes/her* genes are key targets of the Notch signaling pathway and form the central components of the cellular oscillators that control somite formation (Takke and Campos-Ortega, 1999; Bessho et al, 2001; Kageyama et al, 2007). In various species, these genes have been shown to oscillate due to a delayed autoinhibition (Krol et al, 2011; Hirata et al 2002; Oates and Ho 2002; Lewis 2003). In zebrafish, the amplitude and the period of *her* oscillations increase in time as the cells move from the posterior to the anterior part of the PSM (Delaune et al, 2012; Shih et al, 2015). Interestingly, this temporal increase in period and amplitude correlates with the temporal decrease of Fgf and Wnt signaling due to mRNA degradation. Moreover, Fgf and Wnt signaling have been shown to modulate the properties of Hes/her oscillators (Niwa et al, 2007; Kawamura et al, 2005; Wiedermann et al, 2015). This suggests a possible link between the gradient of Fgf/Wnt signaling and the properties of

Hes/her oscillators, where the temporal decay in Fgf/Wnt signaling due to mRNA degradation leads to a temporal increase in the period and amplitude of Hes/her oscillations.

A set of neighboring oscillators with slight differences in period and amplitude are known to lead to travelling waves. This can be visualized in a pendulum wave experiment, where a set of pendulums with gradually increased lengths that start from the same initial condition display a travelling wave (Berg, 1991; Flaten and Parendo, 2001). This is a result of the temporal accumulation of differences in the levels of neighboring oscillators. Inspired by this mechanism, we propose that positional information during somite formation is encoded by the differential levels of neighboring Hes/her oscillators. When the cells are generated in the tail bud region, they start with the same initial condition and Hes/her oscillations are synchronized with their neighbors. As the cells leave the tail bud region and cross the PSM, a temporal increase in the period and amplitude of Hes/her oscillations leads to a gradual increase in the difference of Hes/her levels in neighboring cells. We propose that the differential levels between neighboring oscillators represent the positional value that encodes the information required to start the segmentation program. In order to explore this mechanism, we first develop a theoretical framework. We then show that our model quantitatively fits *in vivo* segmentation from wild type and growth-perturbed embryos, captures temperature compensation in somite size and predicts a delayed scaling between somite size and PSM length. We further use data from different species to suggest possible developmental mechanisms of somite size control. Lastly, we quantitatively fit data from *ex vivo* explants, showing that the proposed mechanism can in principle explain both *in vivo* and *ex vivo* segmentation.

## Results

### Theoretical framework

In our framework, we consider that each cell expresses an oscillatory protein *u* that represents a member of the Hes/her family. For simplicity, we represent the levels of *u* by a sine function:

$$u = A(x,t)\sin\varphi(x,t),$$

where the amplitude *A* and the phase φ depend on the position of the cell *x* and the time *t*.

We consider that each cell has a fixed position *x,* while the tail bud moves in direction of increasing *x*. At the time point $t_0 = t_0(x)$, the cell in position *x* is incorporated into the PSM and the amount of time since the cell was incorporated into the tissue is given by $\Delta t = t - t_0$ (Figure 1). We further define the phase φ of the cellular oscillator by:

$$\varphi = \omega(x,t)\,\Delta t + \varphi_0,$$

where ω is the frequency of oscillation and $\varphi_0 = \omega_0 t_0$ represents the initial phase of the cell with $\omega_0$ being the frequency of the oscillator at the tail bud.

After leaving the tail bud region, the amplitude and period of the oscillations increase over time in the PSM cells (Delaune et al, 2012; Shih et al, 2015). We assume that the increase in the period and amplitude is given by the temporal decrease of Fgf/Wnt signal due to the gradient by inheritance. For convenience, we assume that the increase in the amplitude (A) and period (T) can be mathematically represented by exponential functions:

$$A = A_0 e^{\frac{\Delta t}{\alpha}}$$

$$T = T_0 e^{\frac{\Delta t}{\beta}}$$

where $A_0$ and $T_0$ are the amplitude and period at the tail bud region, respectively, and α and β are the characteristic time scale of amplitude and period gradients, respectively.

The slight difference in period and amplitude between neighboring cells leads to the temporal accumulation of differences in their expression levels. We propose that segmentation occurs when these differences reach a certain threshold (θ). This can be represented mathematically as:

$$\frac{\partial u}{\partial x} = \theta.$$

The derivative of *u* can be written as:

$$\frac{\partial u}{\partial x} = \frac{\partial u}{\partial A}\frac{\partial A}{\partial x} + \frac{\partial u}{\partial \varphi}\frac{\partial \varphi}{\partial x},$$

which leads to:

$$\frac{\partial u}{\partial x} = \sin\varphi \frac{\partial A}{\partial x} + A\cos\varphi \frac{\partial \varphi}{\partial x}.$$

By calculating the spatial derivative of *A* and φ, we have:

$$\frac{A}{g_{t0}}\left[\left(\frac{\omega \Delta t}{\beta}\cos\varphi - \frac{1}{\alpha}\sin\varphi\right) + (\omega_0 - \omega)\cos\varphi\right] = \theta.$$

Using the previous equation, the segmentation points can be inferred computationally. Note that if we assume that $A_0$ is constant during the segmentation process, this parameter can be incorporated into the threshold θ. Therefore, our model has only 5 parameters: the characteristic time scale of the amplitude gradient (α), the characteristic time scale of the period gradient (β), the tail bud growth rate ($g_{t0}$), the oscillation period at the tail bud ($T_0$) and

the normalized threshold ($\theta/A_0$). Note that the segmentation mechanism is dependent on the tail bud growth rate at the time the cells are in the tail bud region ($g_{t0}$). Consequently, after the cells leave the tail bud, all parameters are defined and only Δt changes. This leads to a timer mechanism of somite formation, independent of any spatial input.

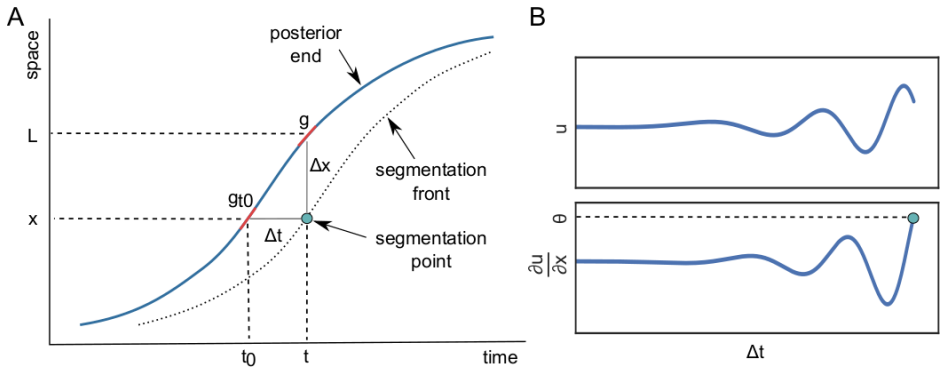


***Figure 1. Schematic representation of segmentation process.*** *A) Blue curve represents the position of the posterior end in time, the green dot represents the segmentation point where du/dx=θ. Δt=t-$t_0$ represents the amount of time since the cell at position x was incorporated to the tissue and Δx=L-x is the distance of the cell x to the posterior end at the time t. The tail bud growth rates $g_{t0}$ and g represent the growth rate at the tail bud at the time $t_0$ and t, respectively. Note that $t_0 = t_0(x)$ such that $\frac{dt_0}{dx} = \frac{1}{g_{t0}}$. B) The amplitude and period of u increases over time, leading to an increase of du/dx until reaching a threshold θ at which segmentation occurs.*

**Disturbed growth affects signaling gradients.**

The segmentation of the vertebrate body is a highly dynamic process. The axial growth rate, the somite size, and the PSM length have been shown to vary broadly during embryonic development and are disturbed in animals that suffered drastic size reduction due to treatment with DNA-synthesis inhibitor Mitomycin C (MMC) (Tam 1981). During mouse somitogenesis, the axial growth rate presents a hump-shaped curve, an initial increase followed by a consecutive decrease (Tam 1981, Figure S1). As a consequence of such growth profile, the axial length increases in a sigmoid-like fashion during development (Tam 1981, Figure S1). Interestingly, although growth-perturbed (MMC-treated) embryos are significantly smaller than wild type (WT) at early stages, these embryos show compensatory growth, resulting in an embryo with normal final size (Tam 1981, Figure S1). Such compensatory growth, however, leads to a disturbed somitogenesis where both the PSM length and somite size are smaller compared to WT embryos (Tam 1981, Figure S2).

Using published experimental data from WT and MMC-treated embryos (Tam 1981), we tested if our model is able to correctly reproduce somite size and PSM length at different

embryonic stages. For simplicity, we decided to keep all parameters fixed during the segmentation process, except the tail bud growth rate, which is highly dynamic and was inferred from experimental data (Tam 1981, Figures 2A,B and S1). However, we observed that segmentation period is also dynamic during mouse somitogenesis (Tam 1981, Figure S3), suggesting that the period of the oscillators changes during this process. One of the key assumptions of our model is that the period and amplitude of the oscillators are dependent on the levels of Fgf/Wnt signal. In this case, we would expect the levels of Fgf/Wnt signal to be dynamic during the segmentation process. Since recent evidences have linked the levels of Fgf to the proliferation rate of PSM cells (Amin et al, 2016), we assumed that the levels of Fgf are proportional to the tail bud growth rate. In this case, the amplitude and period of the oscillations at the tail bud can be considered as a function of the tail bud growth rate, such as:

$$A_0 = A'_0 e^{-\frac{g_{t0}}{\gamma}}$$

$$T_0 = T'_0 e^{-\frac{g_{t0}}{\gamma}},$$

where $g_{t0}$ is the growth rate when the cell is at the tail bud (at $t = t_0$), and γ is a constant. We observed that the inclusion of the parameter γ leads to an improved fit of the segmentation period (Supplementary Information, Figure S3), and a perturbation analysis suggest that this parameter has little effect on somite size and PSM length (Supplementary Information, Figure S4). Using this formulation, we then were able to keep all parameters fixed while only the tail bud growth rate changes during the segmentation process.

We next used the inferred tail bud growth rate as an input to our model and determined the set of parameters that yield the best fit of the model to the PSM length and somite size measured experimentally (Tam 1981). We obtained a good quantitative fit for both experimental conditions (Figures 2C-F). However, we observed that the difference in the growth rate between WT and MMC-treated embryos alone is not enough to explain the differences in somite size and PSM length between these two conditions, and that the characteristic time scale of the amplitude gradient ($\alpha$) is the parameter that changes the most between these conditions (Figure 2G).

These results suggest that our framework is able to quantitatively reproduce mouse segmentation *in vivo* and that modulations in the growth rate additionally affect the characteristic time scale of the amplitude gradient, suggesting a link between the growth rate and the properties of the cellular oscillators, which is likely to be modulated by Fgf signaling.

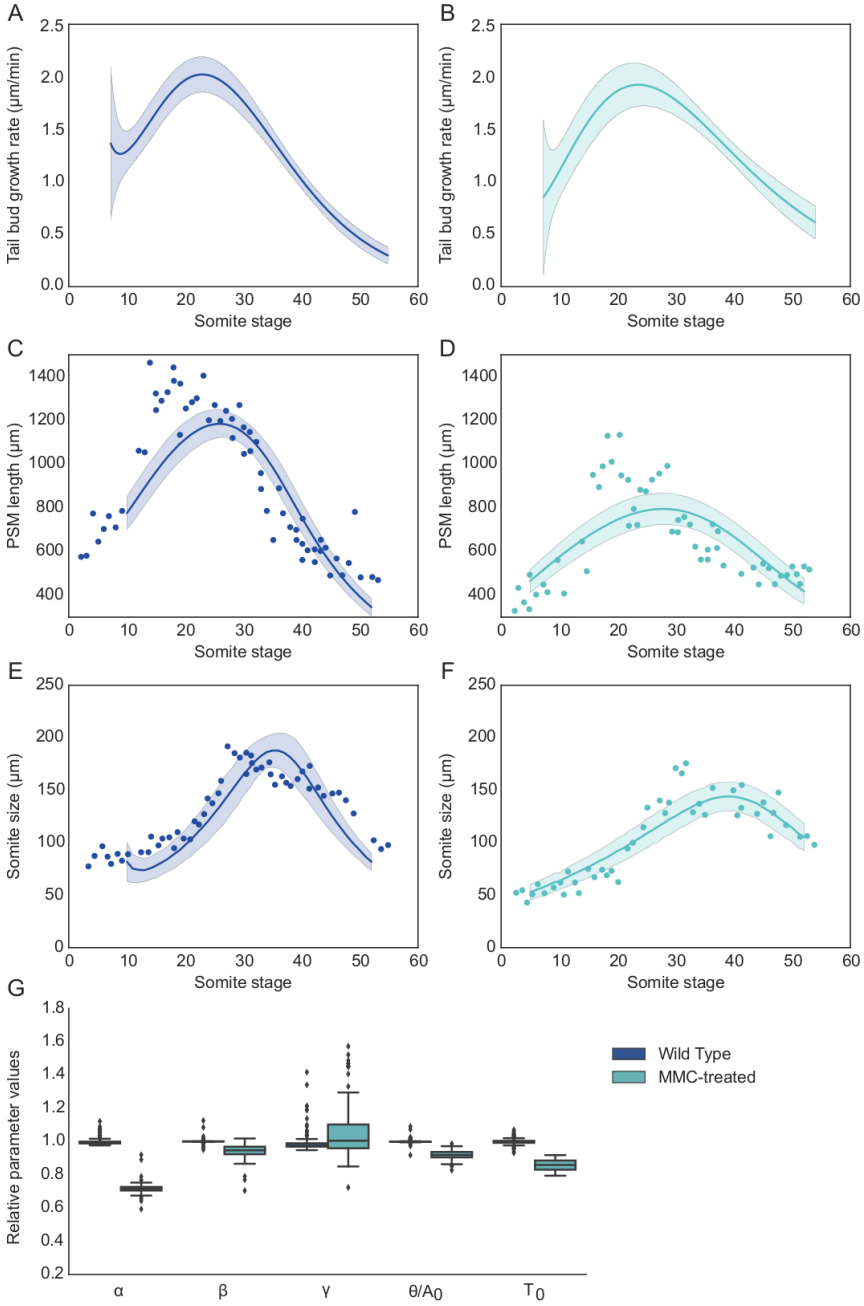


***Figure 2. Properties of mouse segmentation in WT and MMC-treated embryos.*** *A) Inferred tail bud growth rate for different somite stages of WT and B) MMC-treated embryos. Tail bud growth rates were inferred from experimental data (Tam 1981, Figure S1). Lines represent the average fit of a bootstrap resampling and the area represents the 95% confidence interval. C) PSM length for different somite stages for WT and D) MMC-treated embryos. E) Somite size for different somite stages for WT and F) MMC-treated embryos. C-F) Dots represent data from (Tam 1981), lines represent the average fit and the area represents the 95% confidence interval of the model prediction. A total of 100 simulations were evaluated using different fits of the tail bud growth rate, obtained via bootstrap, as an input. G) Comparison of parameter values that best fit the data for WT and MMC-treated embryos. Values are normalized by the average values of WT embryos, which are presented in Table 1.*

**Somite size is temperature compensated and controlled by tail bud growth rate and clock period.**

In the previous section, we observed that our framework is able to reproduce data from *in vivo* mouse segmentation. In order to gain a better understanding of the properties of our model, we considered a simplified case where the tail bud growth rate is constant ($g$). This leads to a stationary state where the PSM length and somite size does not change during the segmentation process (Figure 3A,B). We then performed a perturbation on the values of each parameter to identify the key parameters. We observed that PSM length, somite size and segmentation period are controlled mostly by three key parameters: the tail bud growth rate ($g$), the oscillation period at the tail bud ($T_0$), and the characteristic length of the amplitude gradient ($\alpha$). We found that $g$ positively regulates both PSM length and somite size, $T_0$ positively regulates both the somite size and segmentation period, and $\alpha$ positively regulates the PSM length (Figure 3C).

According to our model, the size of the somite is proportional to the tail bud growth rate and oscillation period (Figure 3C). It is interesting to note that although growth rates and oscillation periods change broadly with the temperature, somite size is the same for embryos grown at different temperatures (Oates et al, 2012). In order to evaluate the conditions to obtain a temperature compensation of somite size, we simulated the segmentation process for different values of growth rates and oscillation periods at the tail bud (Figure 3D). We found that a decrease in the oscillation period can compensate larger somite sizes due to increased growth rates (Figure 3D). Thus, our model suggests a temperature compensation mechanism of somite size. This mechanism is consistent with experimental observations in zebrafish showing that both the somitogenesis frequency and the growth rate increase with the temperature, without altering the size of the somites (Schröter et al, 2008, Oates et al, 2012).

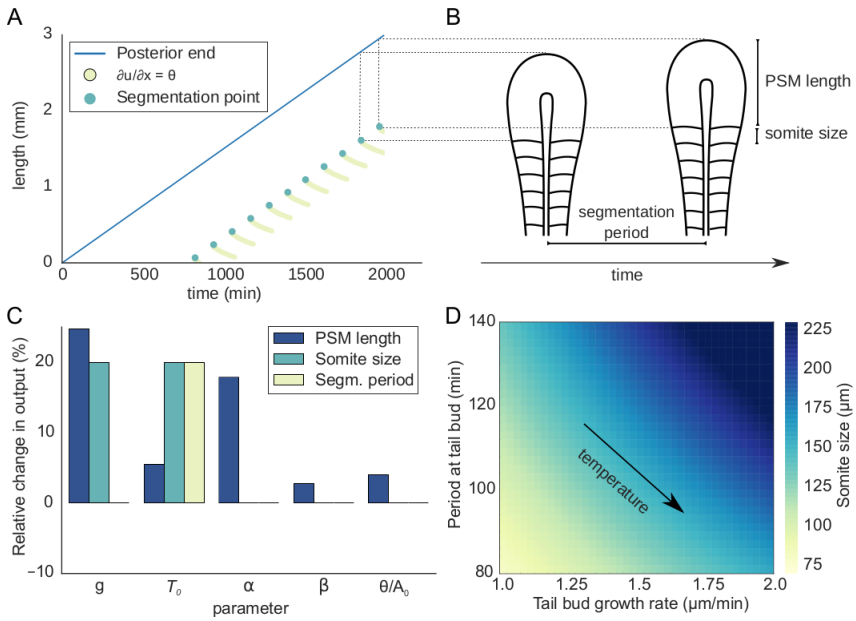


***Figure 3. Segmentation properties at constant tail bud growth rate**. A) Position of posterior end (blue line) and segmentation points in time. Yellow dots represent the points where $\partial u/\partial x = \theta$ and green dots represent where a new segment is formed. The formation of a new segment happens when $\partial u/\partial x = \theta$ is satisfied in a position x such that $x > x_s$, where $x_s$ is the position of the previous segment. B) Graphical representation of segmentation process. Assuming constant tail bud growth rate, the PSM lengthening is exactly the size of one somite during one segmentation period. C) Parameter sensitive analysis. Each parameter is increased in 20% of its standard value (Table 1). The tail bud growth rate (g), clock period at posterior end ($T_0$), and the characteristic length of amplitude gradient (α) are the most sensitive parameters, i.e., lead to changes of more than 10% of either PSM length, somite size and segmentation period. PSM length is regulated by both g and α, somite size is regulated by both g and $T_0$, and segmentation period is controlled by $T_0$. D) Somite size for different values of $T_0$ and g. If an increase in g is accompanied by a proportional decrease in $T_0$, the size of somites remains the same, suggesting a temperature compensation mechanism.*

**Somite size is determined at the tail bud.**

The size of the somites scale with body size (Cooke 1975) and *ex vivo* explants have shown that segment size scales with mPSM size (Lauschke et al, 2013). Nevertheless, the exact relationship between somite size and PSM length is still unclear and a topic of debate.

In measurements of mouse segmentation (Tam 1981, Figure 2), we observe that the growth rate, PSM length and somite size have a similar profile: an initial increase until reaching a peak to further decrease. Moreover, the peak of the growth rate coincides approximately with the peak of PSM length, while the peak of the somite size is delayed in relation to growth rate and PSM length (Tam 1981, Figures S1,2). The delayed relationship between the somite size

with the PSM length and growth rate is intriguing and suggests that the size of the somites is determined before somite formation. Indeed it has been suggested that in zebrafish the determination front is defined a few somite stages before segmentation occurs (Akiyama et al, 2014). Moreover, it has been shown that PSM cells in mouse are organized into segmental units before segmentation (Tam 1981).

How early is the segment size defined? Our model assumes a timer mechanism of somite segmentation rather than a positionally controlled segmentation front. Consequently, in our framework, the segment size would be determined as soon as the cells leave the tail bud region. In order to better illustrate this property, we analyzed our model by considering that the tail bud growth rate presents a hump-shaped curve (Figure 4A), similar to what is observed during mouse segmentation (Tam 1981, Figure 2A,B). We observed that the PSM length and somite size profiles also have a shape similar to the growth dynamics (Figure 4B). The peak of PSM length approximately coincides with the peak of the tail bud growth rate, while the peak in segment size is delayed by around 7 somite stages (Figure 4B). It is interesting to note that this delay is approximately the averaged ratio between the PSM length (*P*) and the size of the most recently formed somite (*s*) (Figure 4B). This ratio represents a good estimate of the amount of time, in somite stages, that the cells spend to move from the tail bud until being incorporated into a new somite. Therefore, our model predicts that the difference in the peaks of PSM length and somite size is the amount of time the cells spend to cross the PSM, which is approximately the ratio *P/s*.

The ratio *P/s* vary significantly between vertebrates. Mouse and chicken has a ratio of around 7-10, while this ratio is around 10-15 in zebrafish and more than 30 in snakes (Gomez et al, 2008). Interestingly, chicken and snakes also present a peak in somite size and PSM length during the segmentation process, while in zebrafish the PSM length decreases during the whole process (Gomez et al, 2008). We then compared the difference in the peaks of somite size and PSM length for mouse, chicken and snakes, and we observed that this difference is approximately the ratio *P/s* (Figure 4C, Gomez et al, 2008).

These results support the idea that the size of the somites depends on the growth rate at the time the cells are at the tail bud. Therefore, according to our model, somite size depends on both the period of oscillation and the tail bud growth rate at the time the cells leave the tail bud region, which can be mathematically represented as:

$$s \approx g_{t0}\, T_0,$$

where $g_{t0}$ is the tail bud growth rate at the time the cells leave the tail bud region ($t = t_0$).

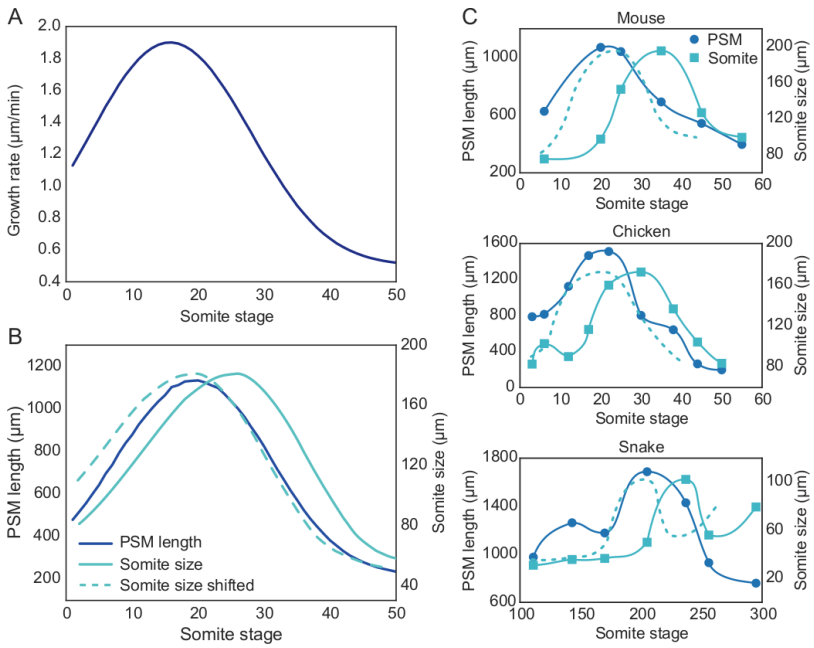


***Figure 4. Relationship between tail bud growth rate, somite size and PSM length for dynamic growth rates.*** *A) Tail bud growth rate for different somite stages. B) Inferred PSM length (blue curve) and somite size (green curve) for the tail bud growth rate presented in A) and with parameters consistent with mouse segmentation (Table 1). The dashed green line represents the somite size curve shifted by the ratio PSM/somite size at the somite stage when PSM length is maximum. C) Experimental measurements of PSM length and somite size during different embryonic stages for mouse, chicken and snake obtained from (Gomez et al, 2008). The dashed curve represents the somite size curve shifted by the ratio PSM/somite size at the somite stage when PSM length is maximum.*

**Evolutionary mechanisms of vertebrate segmentation.**

There is a large diversity in somite size, number and frequency among vertebrate species, but little is known about the evolutionary mechanisms that lead to such diversity (Gomez et al, 2009). For example, while mouse and chicken share similar segmentation properties, snakes and zebrafish have somites three to four times smaller (Figure 5A). Interestingly, snakes and zebrafish achieve smaller somites via different mechanisms. In zebrafish, smaller somites are mostly due to a decrease in the period of oscillations, while snakes have smaller somites due to slower growth rates (Gomez et al, 2008; Figure 5A). This suggests that differences in the growth rate and period of oscillations are the main evolutionary mechanism to achieve somites with different sizes. But are the changes in these parameters sufficient to explain segmentation properties of these different species? To answer that, we used our model to estimate somite size and PSM length for different values of growth rate and oscillation period in the tail bud. We found that changes in these parameters alone are sufficient to explain somite size, but not the observed PSM length (Figure S5).

We further asked if concomitant changes in the characteristic length of the gradients (α and β) could explain changes in both somite size and PSM length. Experimental measurements have shown that the increase in the period from posterior to anterior scales with PSM length in a similar fashion between snakes and zebrafish (Gomez et al, 2008). This suggests that the slowing down of the oscillations from posterior to anterior is similar between different species. Therefore, we expect that the ratio between the period at anterior and posterior part of the PSM to be similar for different species, such that:

$$\left(\frac{T_{ant}}{T_0}\right)_{specie_1} = \left(\frac{T_{ant}}{T_0}\right)_{specie_2}.$$

Consequently:

$$\left(e^{-\frac{\tau}{\beta}}\right)_{specie_1} = \left(e^{-\frac{\tau}{\beta}}\right)_{specie_2},$$

which leads to:

$$\frac{\beta_1}{\beta_2} = \frac{\tau_1}{\tau_2}.$$

Therefore the ratio between the characteristic time scale of the period gradient (β) in different species is proportional to the ratio between the amount of time the cells take to cross the PSM (τ). This amount of time is proportional to the ratio between PSM length and somite size, and can be estimated as:

$$\tau \approx \frac{P}{s}\, T_0.$$

It is interesting to note that both zebrafish and snakes present a higher PSM/somite (P/s) ratio than mouse and chicken. Moreover, this ratio correlates with changes in the tail bud growth rate (*g*), therefore suggesting a possible link between the growth rates and the ratio PSM/somite size (Figure 5B). Using data from different species, we inferred the following relationship between *P/s* and *g* (Figure 5B):

$$\frac{P}{s} \sim g^{-1.5}.$$

Taken together, we can estimate the inter-species ratio of the characteristic length of the period as a function of changes in the growth rate and period at the tail bud:

$$\frac{\beta_1}{\beta_2} = \frac{(g^{-1.5}\, T_0)_1}{(g^{-1.5}\, T_0)_2}.$$

Assuming that the inter-species ratio of the characteristic length of the amplitude follows the same relationship, we have:

$$\frac{\alpha_1}{\alpha_2} = \frac{(g^{-1.5}\, T_0)_1}{(g^{-1.5}\, T_0)_2}.$$

Once we have previously inferred the values of α and β from experimental data for the mouse (Figure 2, Table 1), we took this species as a reference to infer these parameters for other species. We then used our model to estimate the somite size and PSM length for different species and observed that our model correctly captures these values for mouse, chicken, snake and zebrafish (Figure 5C-D). We also observed that snakes show a much larger number of stripes of the oscillatory protein in the PSM than zebrafish, mouse and chicken, which is consistent to experimental observations (Figure 5E, Gomez et al, 2009).

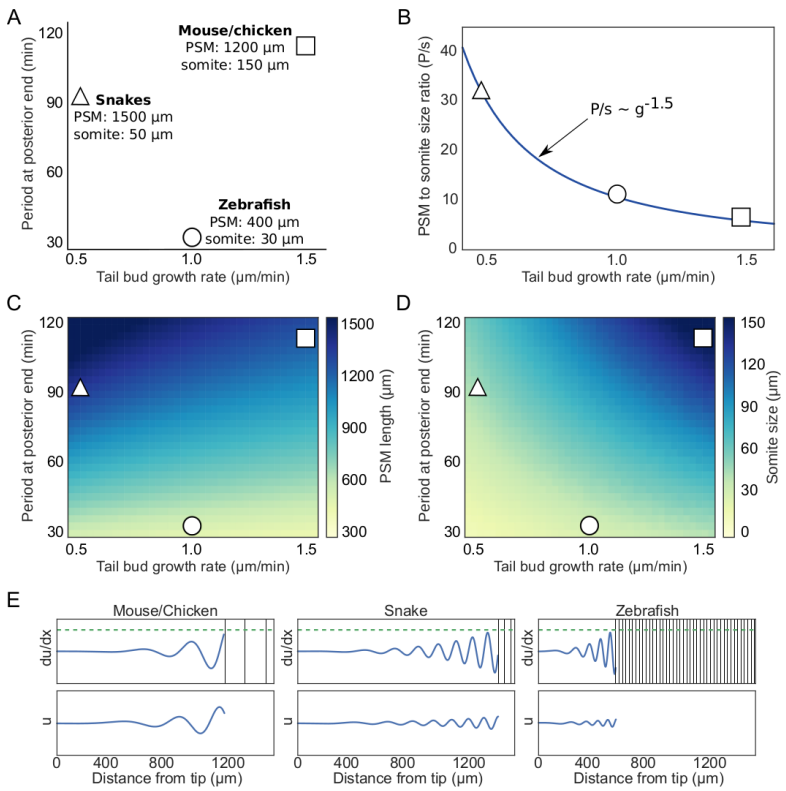


***Figure 5. Segmentation properties of different vertebrate species.*** *A) Representation of the estimated overall growth rate and period in the tail bud, PSM length and somite size for mouse and chicken, snakes and zebrafish (Gomez et al, 2008). B) Relationship between PSM/somite size ratio (P/s) and the tail bud growth rate for different species. Blue line represents the fit that relates the ratio P/s to the growth rate. C) PSM length and D) somite size for different values of growth rate and period at the tail bud. We considered that changes in the growth rate and the period of oscillations also affect the steepness of the gradients. E) Representation of the values of u and* $\partial u/\partial x$ *for different species. Dashed green lines represents the threshold θ, while dark vertical lines represents the position of formed segments.*

**Pattern scaling of ex vivo explants with different temperatures.**

One interesting property of cells from the PSM is the ability to self-organize into emergent monolayer PSM (mPSM) structures when explanted *in vitro* (Lauschke et al, 2013, Tsiairis and Aulehla 2016). These structures show many properties that resemble *in vivo* segmentation, such as the formation of Fgf/Wnt gradients and patterning, although how the cells self-organize into such a spatial structure is still unclear (Lauschke et al, 2013, Tsiairis and Aulehla 2016). One of the most interesting properties of these explants is that the segments are formed proportionally to the mPSM size (Lauschke et al, 2013).

During *in vivo* segmentation, the levels of Fgf and Wnt decrease temporally as the cells cross the PSM due to the gradient by inheritance (Dubrulle and Pourquié 2004, Aulehla et al, 2003). In contrast, during *ex vivo* segmentation, the cells have a fixed position in relation to the center of the mPSM and the gradient is formed from center to periphery (Lauschke et al, 2013, Tsiairis and Aulehla 2016). Therefore, *ex vivo* explants offer a good experimental setup to study the behavior of PSM cells when the gradient is spatially formed. To take this into account, we adapted our model by considering that the amplitude and the period gradient change spatially:

$$A = A_0 e^{\frac{\Delta x}{\alpha'}}$$

$$T = T_0 e^{\frac{\Delta x}{\beta'}},$$

where α' and β' are the characteristic spatial length of the amplitude and period gradients, respectively, and $\Delta x = L - x$, is the distance of the cell x to the center of the mPSM ($L$). In this case, segmentation points can be determined by:

$$A\left[\frac{\omega \Delta t}{\beta'}\cos\varphi - \frac{1}{\alpha'}\sin\varphi\right] = \theta.$$

We then used this framework to fit the relationship between somite size and wave velocity with PSM length for explants at different temperatures (Figure 6A-D, Lauschke et al, 2013). We observed that most parameters have a similar value, with the exception of the period of oscillations, which is longer for explants at lower temperature (Figure 6E). This is consistent with experimental measurements showing that explants at lower temperature have a longer overall oscillation period (Figure 6F, Lauschke et al, 2013).

Taken together, these results suggest that our framework is able to reproduce somite formation from both *in vivo* and *ex vivo* data. The critical difference between both cases is that a spatial gradient self-emerge in *ex vivo* explants, leading to a scaling of segment size with the mPSM, whereas *in vivo*, the tail bud growth controls the delayed scaling between somite size and PSM length.

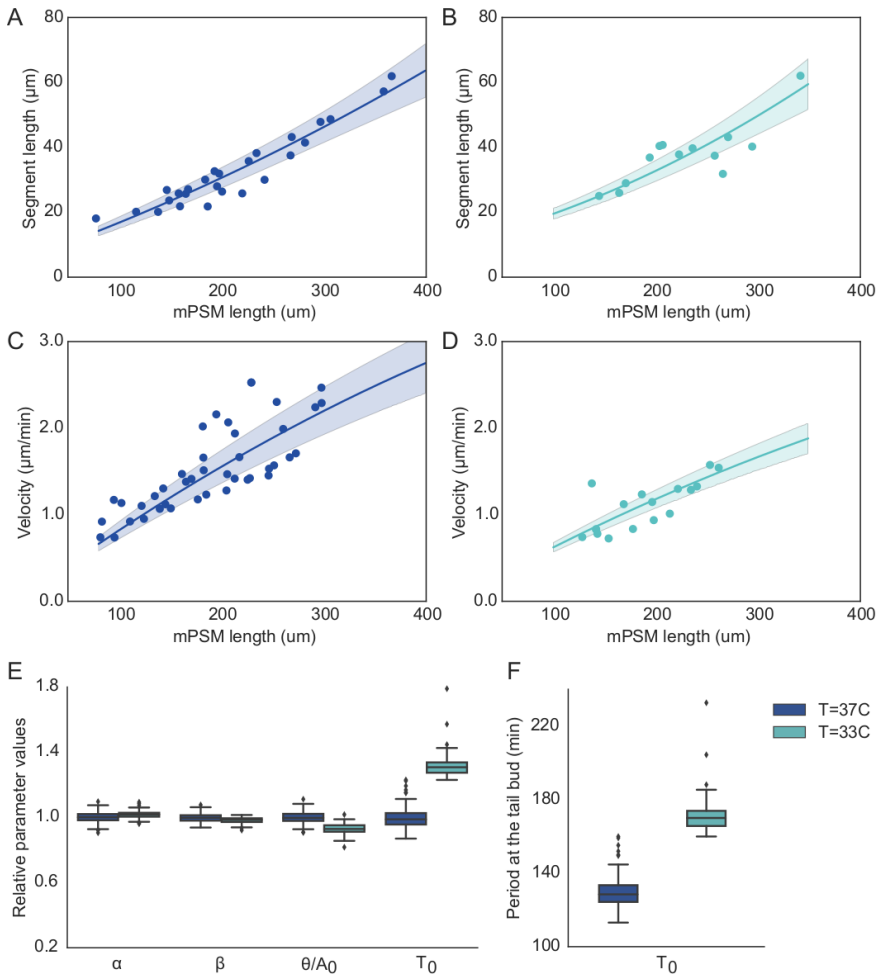


***Figure 6. Properties of mouse segmentation in ex vivo explants at different temperatures.*** *A) Segment size and mPSM length for explants at 37°C and B) 33°C. C) Wave velocity and PSM length for explants at 37°C and D) 33°C. The wave velocity is defined by the mPSM divided by the time to form the segment. A-D) Dots represent data from (Lauschke et al, 2013), lines represent the average fit and area represent the 95% confidence interval of the model prediction. E) Comparison of parameter values that best fit the data for explants at temperatures 37°C and 33°C. The values are normalized by the average values of explants at 37°C. Changes in the period at the center of the mPSM ($T_0$) are required to fit explants from different temperatures. F) The predicted periods are consistent to experimental observations of an overall period of 137.4 and 193.4 min for explants at 37°C and 33°C (Lauschke et al, 2013). Note that since the period increases from the center of the explant to the border, the overall period is expected to be higher than the period at the center.*

## Discussion

How the cells obtain their positional information to coordinate somite formation during vertebrate segmentation is an open question in developmental biology. Over the past decades, the "clock-and-wavefront" model has provided an intuitive conceptual framework to understand *in vivo* somite formation and guided much of the experimental research in the field. Among the successes of this model is the prediction that somite size is dependent on the velocity of tail elongation and the period of oscillations. Nevertheless, in this framework, the clock and the wavefront are considered to be two separated entities and recent experiments with *in vitro* PSM cultures have challenge this idea. When transplanted *in vitro*, PSM cells are able to self-organize into a monolayer (mPSM) and present concentric segmentation that scales with the remaining mPSM (Tsiairis and Aulehla, 2016). These results are difficult to interpret with the 'clock-and-wavefront' model and suggest that the segmentation is independent of long-range regulations and is an intrinsic property of the cellular oscillators (Lauschke et al., 2013; Beaupeux and François, 2016). A phase-difference positional information model has successfully explained segmentation in such explants (Lauschke et al., 2013; Beaupeux and François, 2016) and recent experiments have shown that the phase shift between Notch and Wnt signaling can control segmentation in *ex vivo* explants (Sonnen et al, 2018). Nevertheless, the interpretation of *in vivo* segmentation within this framework is not straightforward.

Here, we propose an alternative approach where somite formation is based on local differences in the levels of neighboring cellular oscillators and that the cells use this relative difference as their positional information. Using this framework, we obtain a good quantitative fit of *in vivo* mouse segmentation in both WT and growth disturbed animals, and *ex vivo* explants at different temperatures. Our model has a relatively simple mathematical formulation with few intuitive parameters that can be measured experimentally. Only three parameters control most of the segmentation properties: the tail bud growth rate, the period of oscillations and the characteristic time scale of the amplitude gradient. In the stationary state, the predictions of our model regarding the regulation of somite size are consistent with the "clock-and-wavefront" mechanism. Somite size is regulated by the tail bud elongation rate (wavefront velocity) and the period of the oscillations, and a concomitant modulation of these parameters due to temperature changes leads to the maintenance of same somite size. Nevertheless, our model differs from the "clock-and-wavefront" model regarding the regulation of PSM length. According to the "clock-and-wavefront" model, the length of the PSM is defined by the signaling wavefront, while in our model the PSM length is mostly dependent on the tail bud growth rate. This is a critical difference. In the "clock-and-wavefront" the shrinkage of the PSM observed in most species requires a dynamic change in the properties of the signaling wavefront, while in our model the reduction of the PSM length can be explained with reduced growth rates. Data from mouse segmentation supports the close relationship between PSM length and tail bud growth rates, therefore favoring the

interpretation from our model (Tam 1981, Figure 2). Our model also makes different predictions regarding when the size of the somites is determined. According to the 'clock-and-wavefront' model, the size of the somites is determined only after the cells cross the wavefront, while in our model, it is determined when the cells are still at the tail bud. Because the size of the somites is defined much earlier, our model predicts a delayed scaling between PSM length and somite size, where the delay is approximately the ratio PSM/somite size. We show that experimental data from different species is in agreement with this prediction. All together, these results support the idea that the somite segmentation program is a timer mechanism that works independent of any long-range signal such as morphogens.

We lastly used our theoretical framework to analyze possible developmental mechanisms of somite size control. According to our model, the tail bud growth rate and the period of the oscillators control the size of the somite, but changes in these parameters alone are not sufficient to explain the PSM length and somite size of different species. We observed that the ratio PSM/somite size varies significantly between different species and by analyzing data from mouse, chicken, snakes and zebrafish, we observed that this ratio correlates with changes in tail bud growth rate. We further inferred a relationship between the characteristic time scale of the amplitude and period gradients (α and β) with the tail bud growth rate. We observed that lower growth rates lead to increased α and β and using this inferred relationship, we correctly reproduced the overall segmentation properties in different species. Our results suggest that segmentation at low growth rates leads to an increased PSM/somite size ratio. Whether such longer PSM as compared to somite size leads to evolutionary advantages is unclear. One possible explanation is that the low growth rate observed in snakes is a consequence of low metabolic rates (Gomez et al, 2008), which would also lead to slower mRNA degradation, therefore leading to an increased time scale of the amplitude and period gradients. In this case, longer PSM length such as observed in snakes are just a consequence of slower metabolism.

Our model makes three key assumptions that require further experimental validation. As the cells cross the PSM, the levels of Fgf and Wnt decrease due to mRNA decay (Dubrulle and Pourquié 2004; Aulehla et al, 2003). Concomitantly, the period and amplitude of Hes/her oscillators increase (Delaune et al, 2012; Shih et al, 2015). Our first assumption is that the increase in period and amplitude of the oscillators is modulated by the temporal decay of Fgf/Wnt gradients. This is a key assumption of our model, as it suggests that the behavior of the oscillators is independent of any spatial information and only time-dependent. Although it has been shown that Fgf and Wnt modulates Hes/her expression (Niwa et al, 2007; Kawamura et al, 2005; Wiedermann et al, 2015), it remains to be confirmed whether decreased Fgf/Wnt levels lead to an increase in Hes/her oscillation period and amplitude in PSM cells. Second, we assume that the tail bud growth rate is dependent on the levels of Fgf at the tail bud, therefore linking the tail bud growth rate with the properties of the oscillators.

This suggests the levels of Fgf would have a similar dynamic as the growth rates. Recent experiments have shown that Fgf modulates growth at the tail bud (Amin et al, 2016), but an experimental comparison of the levels of Fgf at different embryonic stages is still missing. Third, we assume the existence of a molecular mechanism that enables neighboring cells to compare their protein concentration to obtain their positional information. Although there is no explicit molecular evidence of such mechanism, the PSM cells are known to communicate with their neighbors via Notch signaling. Such communication between neighboring cells has been shown to maintain their oscillations synchronized (Jiang et al, 2000) and Notch signaling has been shown to control *Mesp2,* which is required to initiate somite segmentation (Takahashi et al, 2000; Morimoto et al, 2005; Yasuhiko *et al.* 2006). Notch is a versatile signaling pathway (Andersson et al, 2011), but how the cells could use this pathway to both keep their synchronization and read their positional information is unclear and requires further theoretical and experimental investigation.

In summary, we propose a novel mechanism of spatial pattern formation based on the local differences between neighboring oscillators. In our framework, slightly different properties of neighboring oscillators lead to the temporal accumulation of differences in their levels, resulting in travelling waves as observed in a pendulum wave experiment. During vertebrate body segmentation, as the cells flow across the PSM, the oscillations of Hes/her proteins temporally increase in amplitude and period, leading to the accumulation of differences with their neighbors. We propose that the cells use this difference to decode their positional information. It is important to note that this temporal mechanism is different from most patterning mechanism that assume long-range interactions such as morphogen gradients. In our framework, the program of somite formation is already encrypted into the cells before they leave the tail bud region. After that, the cells only need to compare their clock with their neighbor's clock to decide when it is time to form a new segment.

## Material and methods

### Parameter values

***Table1. Parameter values used in the simulations, unless indicated otherwise.***

| Parameters | Figure 2 | Figure 3,4,5 | Figure 6 |
|---|---|---|---|
| α or α' | 158 min | 160 min | 240 μm |
| β or β' | 1208 min | 1200 min | 2470 μm |
| g | from data | 1.5 μm/min | ------ |
| $T_0$ | 80 min | 100 min | 130 min |
| $\vartheta/A_0$ | 1.0 | 1.0 | 0.05 |
| ϒ | 32 min | 30 min | ------ |

### Experimental data

Experimental data was obtained from previous published manuscripts. Data from *in vivo* mouse segmentation was obtained from (Tam 1981), *ex vivo* explants from (Lauschke et al, 2013) and different species from (Gomez et al, 2008). Data were extracted from original manuscripts using WebPlotDigitizer 4.1 online tool (https://apps.automeris.io/wpd/).

### Code availability

The simulations were evaluated in Python and all source codes are presented as Jupyter notebooks (http://jupyter.org/) for easy visualization and are freely available on Github: https://github.com/mboareto/BoaretoTomkalber2018

## References

Akiyama, R., Masuda, M., Tsuge, S., Bessho, Y. and Matsui, T., 2014. An anterior limit of FGF/Erk signal activity marks the earliest future somite boundary in zebrafish. *Development*, *141*(5), pp.1104-1109.

Amin, S., Neijts, R., Simmini, S., van Rooijen, C., Tan, S.C., Kester, L., van Oudenaarden, A., Creyghton, M.P. and Deschamps, J., 2016. Cdx and T brachyury co-activate growth signaling in the embryonic axial progenitor niche. *Cell reports*, *17*(12), pp.3165-3177.

Andersson, E.R., Sandberg, R. and Lendahl, U., 2011. Notch signaling: simplicity in design, versatility in function. *Development*, *138*(17), pp.3593-3612.

Aulehla, A., Wehrle, C., Brand-Saberi, B., Kemler, R., Gossler, A., Kanzler, B. and Herrmann, B.G., 2003. Wnt3a plays a major role in the segmentation clock controlling somitogenesis. *Developmental cell*, *4*(3), pp.395-406.

Beaupeux, M. and François, P., 2016. Positional information from oscillatory phase shifts: insights from in silico evolution. Physical biology, 13(3), p.036009.

Berg, R.E., 1991. Pendulum waves: A demonstration of wave motion using pendula. Am. J. Phys, 59(2), pp.186-187.

Bessho, Y., Sakata, R., Komatsu, S., Shiota, K., Yamada, S. and Kageyama, R., 2001. Dynamic expression and essential functions of Hes7 in somite segmentation. *Genes & development*, *15*(20), pp.2642-2647.

Cooke, J., 1975. Control of somite number during morphogenesis of a vertebrate, Xenopus laevis. *Nature*, *254*(5497), p.196.

Cooke, J. and Zeeman, E. C. 1976. A clock and wavefront model for control of the number of repeated structures during animal morphogenesis. *J. Theor. Biol.* **58**, 455–476.

Delaune, E. A., François, P., Shih, N. P. and Amacher, S. L. (2012). Single-cell-resolution imaging of the impact of Notch signaling and mitosis on segmentation clock dynamics. Dev. Cell 23, 995-1005.

Dequéant, M.L., Glynn, E., Gaudenz, K., Wahl, M., Chen, J., Mushegian, A. and Pourquié, O., 2006. A complex oscillating network of signaling genes underlies the mouse segmentation clock. *science*, *314*(5805), pp.1595-1598.

Dubrulle, J. and Pourquié, O., 2004. fgf8 mRNA decay establishes a gradient that couples axial elongation to patterning in the vertebrate embryo. *Nature*, *427*(6973), p.419.

Dubrulle, J., McGrew, M. J. and Pourquie, O. 2001. FGF signaling controls somite boundary position and regulates segmentation clock control of spatiotemporal Hox gene activation. *Cell* **106**, 219–232.

Flaten, J.A. and Parendo, K.A., 2001. Pendulum waves: A lesson in aliasing. American Journal of Physics, 69(7), pp.778-782.

643 Forsberg, H., Crozet, F. and Brown, N.A., 1998. Waves of mouse Lunatic fringe expression,
644 in four-hour cycles at two-hour intervals, precede somite boundary formation. *Current*
645 *biology*, *8*(18), pp.1027-1030.
646
647 Gomez, C., Özbudak, E.M., Wunderlich, J., Baumann, D., Lewis, J. and Pourquié, O., 2008.
648 Control of segment number in vertebrate embryos. *Nature*, *454*(7202), pp.335-339.
649
650 Gomez, C. and Pourquié, O., 2009. Developmental control of segment numbers in
651 vertebrates. *Journal of Experimental Zoology Part B: Molecular and Developmental*
652 *Evolution*, *312*(6), pp.533-544.
653
654 Hirata, H., Yoshiura, S., Ohtsuka, T., Bessho, Y., Harada, T., Yoshikawa, K. and Kageyama,
655 R. (2002). Oscillatory expression of the bHLH factor Hes1 regulated by a negative feedback
656 loop. Science 298, 840-843. doi:10.1126/science.1074560
657
658 Jiang, Y.J., Aerne, B.L., Smithers, L., Haddon, C., Ish-Horowicz, D. and Lewis, J., 2000.
659 Notch signalling and the synchronization of the somite segmentation clock. Nature,
660 408(6811), p.475.
661
662 Kageyama, R., Ohtsuka, T. and Kobayashi, T., 2007. The Hes gene family: repressors and
663 oscillators that orchestrate embryogenesis. *Development*, *134*(7), pp.1243-1251.
664
665 Kawamura, A., Koshida, S., Hijikata, H., Sakaguchi, T., Kondoh, H. and Takada, S., 2005.
666 Zebrafish hairy/enhancer of split protein links FGF signaling to cyclic gene expression in the
667 periodic segmentation of somites. *Genes & development*, *19*(10), pp.1156-1161.
668
669 Krol, A.J., Roellig, D., Dequéant, M.L., Tassy, O., Glynn, E., Hattem, G., Mushegian, A.,
670 Oates, A.C. and Pourquié, O., 2011. Evolutionary plasticity of segmentation clock networks.
671 Development, 138(13), pp.2783-2792.
672
673 Lauschke, V.M., Tsiairis, C.D., François, P. and Aulehla, A., 2013. Scaling of embryonic
674 patterning based on phase-gradient encoding. *Nature*, *493*(7430), p.101.
675
676 Lewis, J., 2003. Autoinhibition with transcriptional delay: a simple mechanism for the
677 zebrafish somitogenesis oscillator. Current Biology, 13(16), pp.1398-1408.
678
679 McGrew, M.J., Dale, J.K., Fraboulet, S. and Pourquié, O., 1998. The lunatic fringe gene is a
680 target of the molecular clock linked to somite segmentation in avian embryos. *Current*
681 *Biology*, *8*(17), pp.979-982.
682

683 Morimoto, M., Takahashi, Y., Endo, M. & Saga, Y. 2005. The Mesp2 transcription factor
684 establishes segmental borders by suppressing Notch activity. *Nature* **435**, 354–359.
685
686 Naiche, L. A., Holder, N. & Lewandoski, M. 2011. FGF4 and FGF8 comprise the wavefront
687 activity that controls somitogenesis. *Proc. Natl Acad. Sci. USA* **108**, 4018–4023.
688
689 Niwa, Y., Masamizu, Y., Liu, T., Nakayama, R., Deng, C.X. and Kageyama, R., 2007. The
690 initiation and propagation of Hes7 oscillation are cooperatively regulated by Fgf and notch
691 signaling in the somite segmentation clock. *Developmental cell*, *13*(2), pp.298-304.
692
693 Oates, A.C. and Ho, R.K., 2002. Hairy/E (spl)-related (Her) genes are central components of
694 the segmentation oscillator and display redundancy with the Delta/Notch signaling pathway in
695 the formation of anterior segmental boundaries in the zebrafish. Development, 129(12),
696 pp.2929-2946.
697
698 Oates, A.C., Morelli, L.G. and Ares, S., 2012. Patterning embryos with oscillations: structure,
699 function and dynamics of the vertebrate segmentation clock. *Development*, *139*(4), pp.625-
700 639. doi: 10.1242/dev.063735
701
702 Palmeirim, I., Henrique, D., Ish-Horowicz, D. and Pourquié, O. (1997). Avian hairy gene
703 expression identifies a molecular clock linked to vertebrate segmentation and somitogenesis.
704 Cell, 91(5), pp.639-648.
705
706 Sawada, A., Shinya, M., Jiang, Y.J., Kawakami, A., Kuroiwa, A. and Takeda, H., 2001.
707 Fgf/MAPK signalling is a crucial positional cue in somite boundary formation.
708 Development, 128(23), pp.4873-4880.
709
710 Schröter, C., Herrgen, L., Cardona, A., Brouhard, G.J., Feldman, B. and Oates, A.C., 2008.
711 Dynamics of zebrafish somitogenesis. *Developmental Dynamics*, *237*(3), pp.545-553. DOI:
712 10.1002/dvdy.21458
713
714 Sonnen, K.F., Lauschke, V.M., Uraji, J., Falk, H.J., Petersen, Y., Funk, M.C., Beaupeux, M.,
715 François, P., Merten, C.A. and Aulehla, A. (2018). Modulation of Phase Shift between Wnt
716 and Notch Signaling Oscillations Controls Mesoderm Segmentation. Cell, 172(5), pp.1079-
717 1090.
718
719 Shih, N. P., François, P., Delaune, E. A. and Amacher, S. L. (2015). Dynamics of the slowing
720 segmentation clock reveal alternating two-segment periodicity. Development 142, 1785-1793.
721

Takahashi, Y., Koizumi, K.I., Takagi, A., Kitajima, S., Inoue, T., Koseki, H. and Saga, Y., 2000. Mesp2 initiates somite segmentation through the Notch signalling pathway. Nature genetics, 25(4), p.390.

Takke, C. and Campos-Ortega, J.A., 1999. her1, a zebrafish pair-rule like gene, acts downstream of notch signalling to control somite development. *Development*, *126*(13), pp.3005-3014.

Tam, P.P.L., 1981. The control of somitogenesis in mouse embryos. *Development*, *65*(Supplement), pp.103-128.

Tsiairis, C.D. and Aulehla, A., 2016. Self-organization of embryonic genetic oscillators into spatiotemporal wave patterns. *Cell*, *164*(4), pp.656-667.

Yasuhiko, Y. *et al.* 2006. Tbx6-mediated Notch signaling controls somite-specific Mesp2 expression. *Proc. Natl Acad. Sci. USA* **103**, 3651–3656.

Wiedermann, G., Bone, R.A., Silva, J.C., Bjorklund, M., Murray, P.J. and Dale, J.K., 2015. A balance of positive and negative regulators determines the pace of the segmentation clock. eLife, 4.

Wolpert, L., 1969. Positional information and the spatial pattern of cellular differentiation. Journal of theoretical biology, 25(1), pp.1-47.

## Supplementary Information

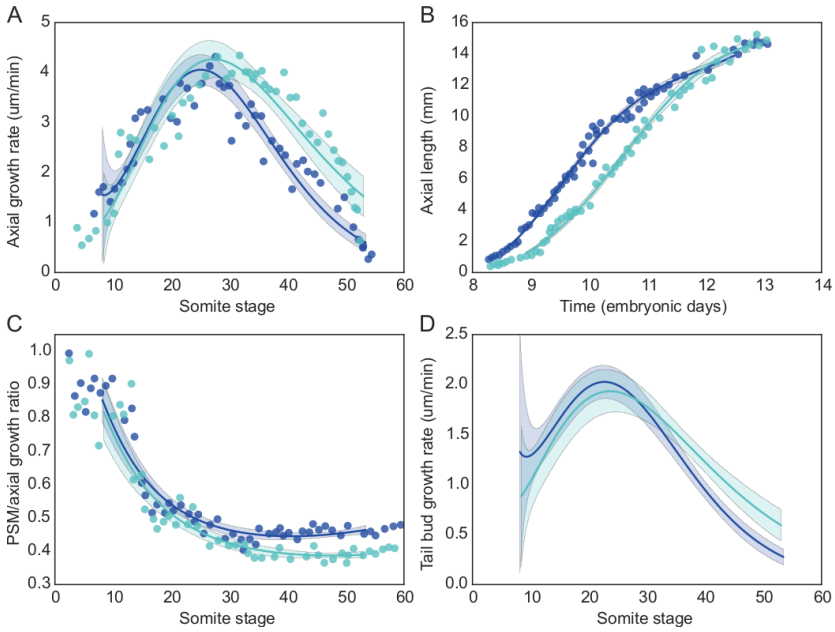


***Figure S1. Growth profiles of WT and MMC-treated embryos.*** *A) Axial growth rate for different somite stages. B) Axial length for different embryonic times. C) Fraction of growth rate due to tail bud elongation for different somite stages. D) Tail bud growth rate for different somite stages inferred by scaling the axial growth rate with the relative growth due to tail bud elongation. A-C) Points represent data from (Tam 1981), solid line represents average fit and area represents 95% confidence interval of a bootstrap fit. Dark blue represents WT and light green represents MMC-treated embryos.*

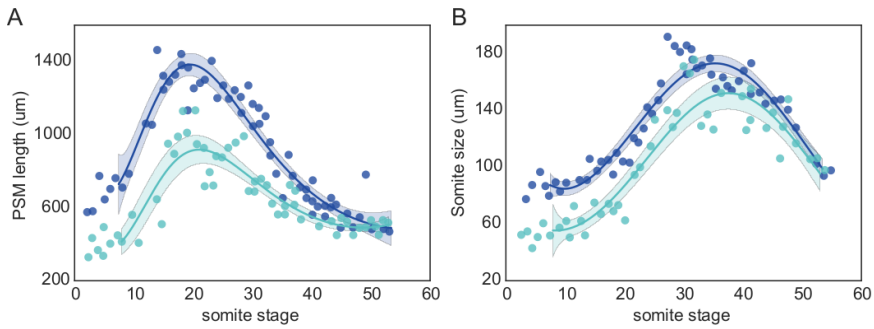


***Figure S2. PSM length and somite size profile of WT and MMC-treated embryos.*** *A) PSM length for different somite stages. B) Somite size for different somite stages. Points represent data from Tam 1981, solid line represents average fit and area represents 95% confidence interval of a bootstrap fit. Dark blue represents WT and light green represents MMC-treated embryos.*

**Model formulation considering dynamic period and amplitude at the tail bud.**

In order to reproduce *in vivo* data, we considered that the amplitude and period of the oscillations at the tail bud are dependent on tail bud growth rate, such as:

$$A_0 = A'_0 e^{-\frac{g_{t0}}{\gamma}}$$

$$T_0 = T'_0 e^{-\frac{g_{t0}}{\gamma}},$$

where $g_{t0}$ is the growth rate when the cell is at the tail bud (at $t = t_0$), and $\gamma$ is a constant. Then, the amplitude and period gradient can be expressed as:

$$A = A'_0 e^{-\frac{g_{t0}}{\gamma}} e^{\frac{\Delta t}{\alpha}}$$

$$T = T'_0 e^{-\frac{g_{t0}}{\gamma}} e^{\frac{\Delta t}{\beta}},$$

and segmentation can be estimated by the following equation:

$$\frac{\partial u}{\partial x} = A\left[\left(\frac{\omega \Delta t}{\beta}\cos\varphi - \frac{1}{\alpha}\sin\varphi + (\omega_0 - \omega)\cos\varphi\right)\frac{1}{g_{t0}} + \left((\omega\Delta t + \omega_0 t_0)\cos\varphi - \sin\varphi\right)\frac{1}{\gamma}\frac{\partial g_{t0}}{\partial x}\right]$$

where $\frac{\partial g_{t0}}{\partial x}$ represents the difference in the growth rate at the tail bud region between neighboring cells, which is expected to be small. This leads to the following simplified expression for obtaining the segmentation points:

$$\frac{A}{g_{t0}}\left[\left(\frac{\omega \Delta t}{\beta}\cos\varphi - \frac{1}{\alpha}\sin\varphi\right) + (\omega_0 - \omega)\cos\varphi\right] = \theta.$$

We noted that assuming a dynamic modulation of the amplitude and period leads to a better overall fit of experimental data (Figure S3) and that perturbations on the values of γ have a little effect on the PSM length, somite size and segmentation period (Figure S4).

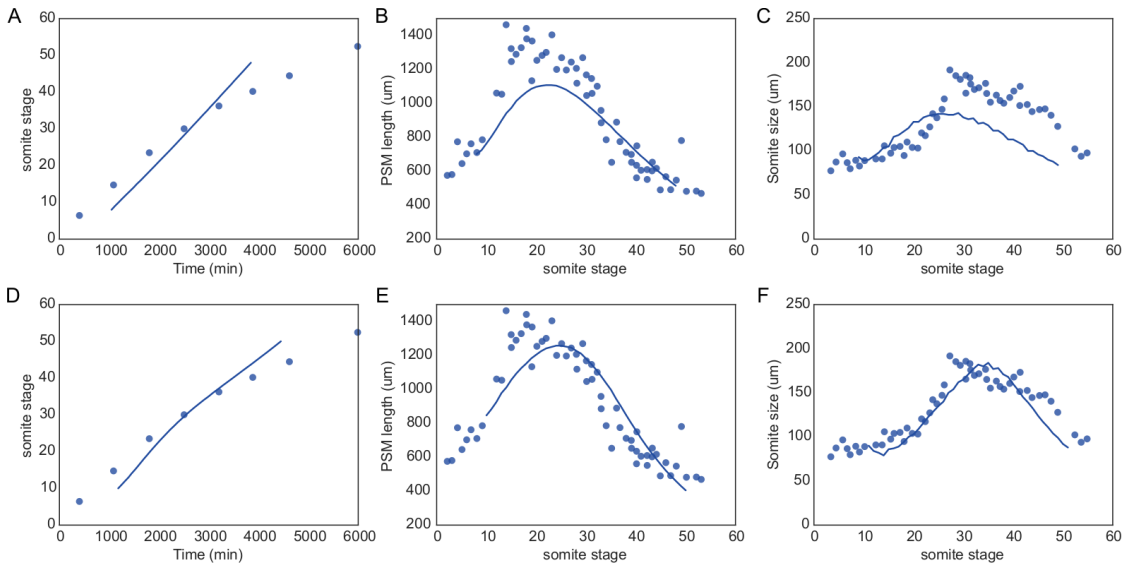


***Figure S3. Fit of mouse* in vivo *segmentation data.*** *A,D) Relationship between somite stage and embryonic time. B-E) PSM length at different somite stages. C,F) Somite size at different somite stages. Circles represent data from (Tam 1981) and lines represent the fit from the modeling using the average value of tail bud growth rate as input. A-C) Modeling results when considering constant period and amplitude at the tail bud. D-F) Modeling results when considering that the period and amplitude at the tail bud are dynamic and dependent on the tail bud growth rate.*

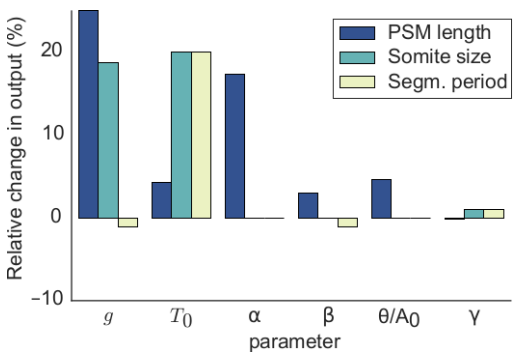


***Figure S4. Sensitive analysis by considering the period and amplitude at the tail bud is dependent on the growth rate.*** *The extra parameter γ has little effect on PSM length, somite size and segmentation period.*

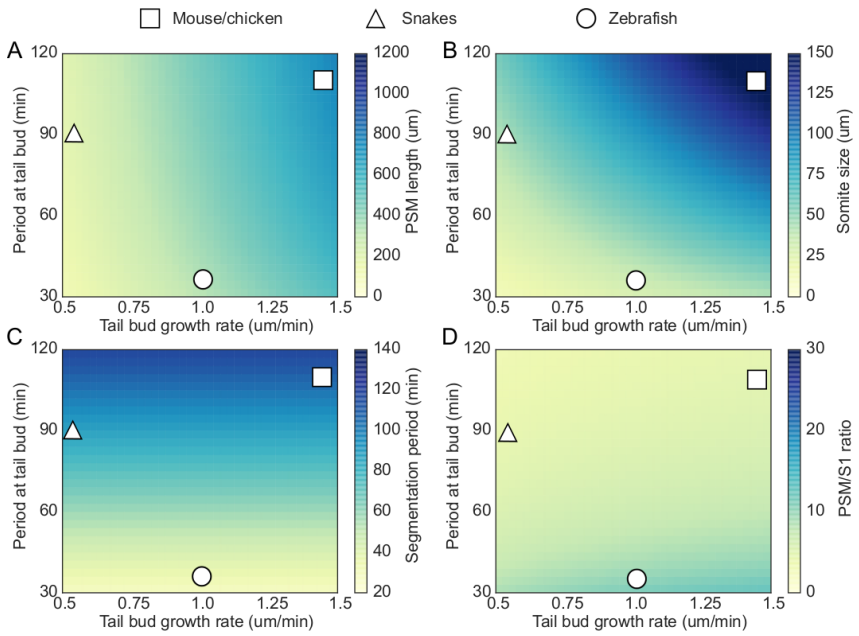


***Figure S5.*** *A) PSM length, B) somite size, C) segmentation period and D) PSM/somite size ratio for different values of growth rate and period at the tail bud. The characteristic length of amplitude and period gradient is remained constant (same values of Figure 3, see Table 1). Note that in this case, our model would predict that snakes would have a much smaller PSM length (around 300 μm). This is in contrast with experimental evidences showing that snakes have a PSM length of around 1200 μm (Gomez et al, 2008).*